JOURNAL OF CATALYSIS 136, 432–445 (1992)

Molybdenum-oxo Species Deposited on Titania by Adsorption: Mechanism of the Adsorption and Characterization of the Calcined Samples

N. SPANOS, H. K. MATRALIS, CH. KORDULIS, AND A. LYCOURGHIOTIS[1]

Department of Chemistry and the Institute of Chemical Engineering and Chemical Processes at High Temperatures, P.O. Box 1239, University Campus, GR-26110 Patras, Greece

Received August 13, 1991; revised February 6, 1992

The mechanism of the adsorption of molybdates on the titania surface has been investigated using adsorption equilibrium experiments, potentiometric titrations, and microelectrophoretic mobility measurements. Comparison of adsorption data with the surface charge of titania, regulated by changing the pH of the impregnating solution, demonstrated that the groups responsible for the creation of the adsorption sites are mainly the protonated surface hydroxyls of titania in addition to the neutral sites. Moreover, the results obtained by the combination of potentiometric titrations and microelectrophoretic mobility measurements, and the variation of pH before and after adsorption with the $Mo^{(VI)}$ concentration suggested that the MoO_4^{2-} ions are adsorbed on the Inner Helmholtz Plane (IHP) of the electrical double layer, which is developed between the surface of the titania particles and the impregnating solution. Finally, from the analysis of the isotherms obtained it was concluded that the adsorbed MoO_4^{2-} ions are located on energetically equivalent sites of the IHP and that relatively weak lateral interactions are exerted. On the basis of the above-mentioned mechanism, an explanation of the dependence of the sorptive capacity of titania on the pH of the impregnating solution is provided. The combined use of NO and CO_2 adsorption, as well as XPS, RAMAN spectroscopy, and temperature programmed reduction measurements, showed that at pH 7.3, corresponding to about 2 wt% MoO_3, the titania surfaceis completely covered and the active surface reaches its maximum value. At pH values lower than 7.3, a second molybdena layer starts to form until the MoO_3 content reaches the 5.4 wt% MoO_3, a point at which MoO_3 crystallites are formed.

INTRODUCTION

There is a present-day interest in studying molybdena catalysts supported on industrial carriers [γ-Al_2O_3, TiO_2, SiO_2]. However, relatively few studies dealing with catalysts prepared by equilibrium adsorption followed by filtration are reported in the literature (*1–9*). As a result, the mechanism by which the molybdate ions are deposited on the support surface remains unclear. Since understanding the mechanism of molybdenum uptake on the catalyst support is of key importance in the preparative process of catalysts manufacturing, we have started a program for the investigation of the adsorption mechanism in aqueous suspensions beginning with γ-Al_2O_3 carriers (*7*). This study showed that the deposition of the $Mo^{(VI)}$ on the γ-alumina surface took place via adsorption of the molybdates, mainly of the MoO_4^{2-} ions, on energetically equivalent sites of the Inner Helmholtz Plane of the electrical double layer. The creation of these sites was mainly attributed to the presence of the protonated surface hydroxyls of γ-alumina. Moreover, it was found that considerable lateral interactions were exerted between the adsorbed molybdate species.

In the present work we attempted to clarify the mechanism of adsorption of the molybdates on the surface of titania. The titania used in the present study, identical

[1] To whom correspondence should be addressed.

0021-9517/92 $5.00

with the kind commonly employed in catalysis, is a mixture of two polymorphic phases, namely anatase and rutile. According to the oxide charging mechanism, two sets of equilibria, one for each of the two polymorphic oxides, should be considered (*10*),

$$\mathrm{Ti^rOH_2^+} \overset{K_1^r}{\rightleftharpoons} \mathrm{Ti^rOH} + \mathrm{H_s^{r+}},$$

$$\mathrm{Ti^aOH_2^+} \overset{K_1^a}{\rightleftharpoons} \mathrm{Ti^aOH} + \mathrm{H_s^{a+}}$$

$$\mathrm{Ti^rOH} \overset{K_2^r}{\rightleftharpoons} \mathrm{Ti^rO^-} + \mathrm{H_s^{r+}},$$

$$\mathrm{Ti^aOH} \overset{K_2^a}{\rightleftharpoons} \mathrm{Ti^aO^-} + \mathrm{H_s^{a+}} \quad \text{(a)}$$

$$\mathrm{H_s^{r+}} \rightleftharpoons \mathrm{H_b^+},$$

$$\mathrm{H_s^{a+}} \rightleftharpoons \mathrm{H_b^+},$$

where $TiOH_2^+$, TiO^-, and TiOH represent protonated, deprotonated, and neutral surface hydroxyls, respectively. By H_s^+ and H_b^+ we denote respectively the hydrogen ions on the surface of the support and in the bulk solution. The superscript r stands for rutile and a for anatase. A salient consequence of the fact that titania is actually a mixture of two simple oxides is that it is extremely difficult to calculate the concentration of the charged surface groups for each component. However, the acid–base behavior of this support allows the determination of the total surface charge, σ_0^T, by potentiometric titrations (*10*). This determination in the presence of the molybdate ions was done in the present work. σ_0^T vs pH curves obtained experimentally were used for estimating the relative variation with pH of the concentration of the various surface groups. Moreover, in order to investigate the adsorption mechanism we determined a parameter proportional to the surface charge, namely, the hydrogen ions consumed in the equilibria (a) both in the presence and absence of the molybdates. A second consequence of having both rutile and anatase in our TiO_2 carrier is that two adsorption mechanisms of the molybdates, one for each TiO_2 component, should be considered. But this cannot be done using the method developed in the case of γ-Al_2O_3 (*7*), which is a simple oxide. The only way to overcome this difficulty was to assume that the adsorption equilibria for rutile and for anatase coincide thus allowing the treatment of the oxide as one phase. This assumption seems to be reasonable at room temperature where the point of zero charge of rutile, and thus the values of the acidity constants, are very close to those for anatase (*11*). Reasonably therefore, it was assumed that the molybdates cannot distinguish between the electrical double layers developed on the surface of rutile and anatase.

Based on this assumption, we attempted to clarify the mechanism of the molybdate adsorption on the TiO_2 surface. Specifically, we tried to investigate the following points: (i) The part of the double layer where the molybdate ions are located, i.e., are they located on the surface of the support, at the Inner Helmholtz Plane (IHP), or in the diffuse part of the double layer? It should be noted here that in addressing this question we have used the "triple-layer model" for the electrical double layer (Fig. 1). (ii) The kind of the molybdate species adsorbed. (iii) The existence of lateral interactions between the adsorbed molybdate ions. (iv) The surface groups responsible for the creation of sorptive sites, i.e., answering the question whether they are the deprotonated, the neutral (*3, 5, 12–14*) or the protonated hydroxyls (*1, 2, 4, 6, 15–17*)? Questions (i)—(iv) shown above were tackled by adsorption equilibrium experiments, potentiometric titrations, microelectrophoretic mobility measurements, the variation of pH, before and after adsorption, with the concentration of the $Mo^{(VI)}$, and the mathematical analysis of the adsorption isotherms.

A recently published work reported on MoO_3/TiO_2 catalysts prepared by equilibrium adsorption over a pH range focusing on their structure after calcination (*9*). Although the characterization done was almost complete, the interpretation of the in-

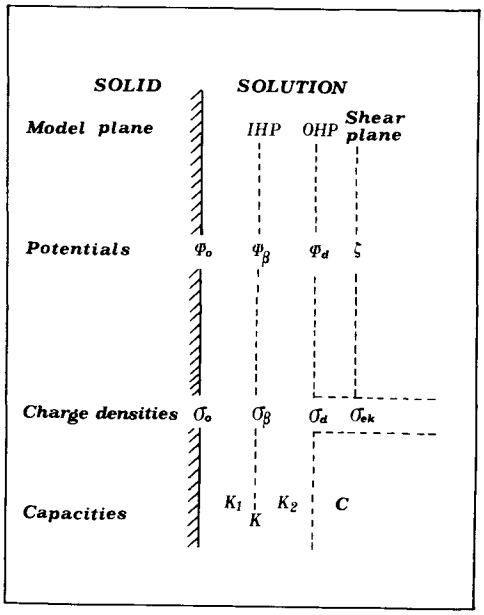

FIG. 1. Structure of the electrical double layer. Triple-layer model.

crease in the $Mo^{(VI)}$ uptake and active surface with decreasing pH was based on the isoelectric point (i.e.p.) of TiO_2. The measurements of the electrokinetic charge presented, however, referred to the shear plane of the double layer and therefore it cannot describe the surface of the titania particles. Only in the special case where specific adsorption does not take place, the i.e.p. is equal to the point of zero charge (p.z.c.) and therefore the microelectrophoretic mobility measurements and the electrokinetic charge calculated may be used for a quite approximative estimation of the concentration of the sorptive sites. In general, however, a more reliable approximation is needed. This was the second task of this work. Specifically, it was attempted to explain the dependence of $Mo^{(VI)}$ uptake on pH in terms of the mechanism of adsorption of the molybdates on the TiO_2 surface. Moreover, a characterization of the MoO_3/TiO_2 catalysts prepared by adsorption was done using BET measurements, NO and CO_2 adsorption, XP and Raman spectroscopy, and temperature programmed reduction.

EXPERIMENTAL

Materials

Commercially available titania (Degussa, P25) was used. The supplier reported a B.E.T. specific surface area of 50 $m^2\ g^{-1}$ and a composition of 20% of rutile and 80 wt% of anatase. The SSA reported was confirmed by B.E.T. measurements in our laboratory. The solid was dried at 120°C for 2.5 h and next it was calcined at 550°C for 5 h. Ammonium heptamolybdate and ammonium nitrate stock solutions were prepared from the corresponding crystalline reagents (Riedel de Haen, both of 99% purity).

Equilibrium Adsorption

Equilibrium adsorption experiments were done at 25.0 ± 0.1°C and over a pH range between 4.6 and 9.0. The range of the molybdate concentrations investigated varied between 6×10^{-4} and 3×10^{-2} mol $(Mo^{(VI)})$ dm^{-3}. The ionic strength, adjusted by ammonium nitrate, was 0.1 mol dm^{-3} and the suspension pH was adjusted by the addition of small aliquots of strong standard acid or base. The surface concentration of $Mo^{(VI)}$, Γ(mol m^{-2}), was computed from the concentration difference before and after adsorption according to

$$\Gamma = \{V(C_0 - C_{eq})\}/WS, \qquad (1)$$

where C_0, C_{eq}, V, W, and S denote, respectively, the $Mo^{(VI)}$ solution concentration before and after adsorption (mol dm^{-3}), the suspension volume (dm^3), the weight (g), and the specific surface area of the carrier ($m^2\ g^{-1}$). Full details regarding the equilibrium adsorption experiments have been reported elsewhere (*7*).

Preparation of the Catalysts

The catalysts were prepared by adsorption of the $Mo_xO_y^{z-}$ ions on the support surface. Specifically, an amount of the TiO_2 powder equal to 7.14 g was suspended into

a molybdate solution of 2×10^{-2} mol $Mo^{(VI)}$ dm^{-3}, volume totalling 2 dm^3. In all preparations the ionic strength of the solution was adjusted to 0.1 mol dm^{-3} by NH_4NO_3. The pH of the suspension was regulated using HNO_3 or NH_4OH. The suspension was kept under stirring at constant temperature (25°C) for 20 h and then it was filtered through membrane filters [Millipore, 0.22 μm]. The filtrate was analyzed spectrophotometrically [Varian Cary 3 UV–Vis] for total molybdenum at 490 nm. The Mo deposited was determined using Eq. (1). The solid was dried at 120°C for 2.5 h. Then it was calcined at 300°C for 1 h and then at 500°C for 5 h.

Microelectrophoresis

Microelectrophoretic mobility measurements on titania suspensions at room temperature allowed for the determination of the electrokinetic charge density, $\sigma^{T}_{e.k.}$, namely, the charge at the shear plane of the double layer. Details on the experimental procedure followed have been reported elsewhere (*7*).

Potentiometric Titrations

The experimental procedure concerning the potentiometric titrations of electrolyte solutions or suspensions has been reported elsewhere (*16, 18*). According to this technique, the electrolyte solution or suspension is titrated using an acid and its pH is recorded every 2 min as a function of the volume of titrant added. The above technique allows the determination of the amount of the hydrogen ions consumed (H_c^+) for the protonation of the surface TiO^-, TiOH groups, as well as in the equilibria taking place in the solution, using the equation

$$H_c^+ = H_{ad}^+ - H_{ac}^+ - H_w^+, \qquad (2)$$

where H_{ad}^+, H_{ac}^+, and H_w^+ represent the amounts of the hydrogen ions added to the solution or suspension, accumulated in the solution or suspension decreasing their pH, and consumed in the equilibrium (b) [$H_2O \rightleftarrows H_b^+ + OH^-$ (b)], respectively. The terms in the right hand side of the above equation may be determined using the relationships

$$H_{ad}^+ = C\,\Delta V \qquad (3)$$

$$H_{ac}^+ = (V + \Delta V)C_{H+} - VC_{H+,in} \qquad (4)$$

$$H_w^+ = VC_{OH-,in} - (V + \Delta V)C_{OH-}, \qquad (5)$$

where C, V, ΔV, C_{H+}, C_{OH-}, $C_{H+,in}$, and $C_{OH-,in}$ represent, respectively, the concentration of the titrant (0.1 N HNO_3), the volume of the solution or suspension before titration, the titrant volume increment, the concentration of the hydrogen and hydroxyl ions in the solution or suspension after its titrant addition, and the corresponding initial concentrations, i.e. before adding titrant.

By determining the value of H_c^+ at suitably selected solutions and suspensions, the hydrogen ions consumed only for the protonation of TiO^- and TiOH groups both in the absence (H_T^+) and presence ($H_{T,Mo}^+$) of the molybdate ions may be determined (see below). By using the values of $H_{T,Mo}^+$ determined at three different ionic strength values and following a procedure reported elsewhere (e.g. (*16, 18*)), we determined the point of zero charge as well as the surface charge at various pH values in the presence of molybdate ions.

Specific Surface Area (SSA) Measurements

The SSA of the catalysts were determined using a well known flow technique. This technique involves the uptake of an adsorbate from a flowing mixture of the adsorbate in an inert gas. Pure nitrogen (Linde special) and helium (Linde 99.996%) were used as adsorbate and inert gas, respectively, in a laboratory constructed apparatus. The amount of nitrogen adsorbed at liquid nitrogen temperature and at three different partial pressures was determined using a thermal conductivity detector of a gas chromatograph (Varian Series 1700).

Adsorption of Nitric Oxide

The dynamic method was used to study chemisorption of nitric oxide. The experiments were performed in laboratory-constructed equipment consisting of three parts: (a) the gas handling system where the gases were purified and the flow rates were adjusted; (b) the adsorption vessel with the possibility of a temperature programmed heating, a six-port valve for injection of nitric oxide pulses, and a four-port valve for precluding any air contamination when the sample was transported from an apparatus to another; (c) a thermal conductivity detector Varian 1700 and an integrator–recorder Shimadzu C-RGA for the determination of the amount of nitric oxide eluted from the adsorption vessel.

A preweighted amount of the oxide catalyst (100 mg) was introduced to the vessel which was then connected via the four-port valve in a sulphidation apparatus. The sulphidation procedure was as follows: The sample temperature was increased up to 400°C with a rate 10°C min^{-1} under argon. Then a mixture of H_2S/H_2 (15 : 85 v/v) was fed for 2.5 h. The amount of adsorbed H_2S remaining after sulphidation was removed by flushing the sample with argon for 1 h at the same temperature. The sample was then cooled down to room temperature and transported to the nitric oxide adsorption equipment where it remained for 1 h under a stream of helium. Pulses of the adsorption mixture [NO-He (5 : 95 v/v)] were introduced every 3 min. The amount of nitric oxide eluted after each injection was measured until two successive pulses gave a difference less than 1%. The total uptake of nitric oxide was thus determined. The catalyst was then maintained for 1 h under a stream of pure helium and the procedure was repeated. The difference in the uptake of nitric oxide during the first and the second adsorption cycle was considered to be equal to the amount of nitric oxide chemisorbed (*19–21*).

Adsorption of Carbon Dioxide

The dynamic method and the equipment used for the nitric oxide chemisorption measurements were also used for determining the amount of CO_2 chemisorbed on the oxide samples. The differences between the procedures followed for determining NO and CO_2 adsorption are the following:

(a) The sulphidation step was replaced in the case of carbon dioxide adsorption by a heating step for 1 h at 150°C under a pure helium stream.

(b) The adsorption mixture was carbon dioxide helium (5 : 95 v/v).

Temperature Programmed Reduction (TPR)

The TPR experiments were performed using the above-mentioned apparatus in which the ideas of the Rogers–Amenomiya–Robertson arrangement (*22*) have been followed. An amount of sample 0.05 g was placed in a quartz reactor and the reducing gas mixture (H_2/Ar : 5/95 v/v) was passed through it for 2 h with a flow rate of 40 ml min^{-1} at room temperature. Then the temperature was increased to 900°C with a constant rate of 12°C min^{-1}. Reduction leads to a decrease of the hydrogen concentration in the gas mixture, which was detected by the thermal conductivity detector. The reducing gas mixture was dried in a cold trap (−95°C) before reaching the katharometer.

Laser Raman Spectroscopy

Laser Raman spectra of the calcined catalysts were obtained using a spectrophotometer involving an Ar^+ ion laser (Spectra Physics, Model 164), a double monochromator (Spex, Model 1403), and a Photon Counting System (Ortec, Model 9302, 9310, 9349). The spectra were obtained at room temperature by using the 514.5 nm excitation line. The power of the beam was 75 mW. The spectral slitwidth was 5 cm^{-1}. The catalyst samples were pressed into the form of pellets at a pressure of about 100 kp cm^{-2}. The sample holder permitted the rotation

of the samples during the recording of the spectra in order to diminish any damage caused by radiation.

X-ray Photoelectron Spectroscopy (XPS)

The XPS analysis was performed at room temperature with a SSX-100 model 206 Surface Science Instruments (SSI) photoelectron spectrometer, interfaced to a Hewlett–Packard 9000/310 computer. The residual pressure in the spectrometer was in the range of 1.3 to 6.5 $\times$ 10^{-7} Pa. A monochromated Al anode (energy of the Alkaline 1486.6 eV) powered at 10 keV and 20 mA was used for X-ray production. The binding energy scale of the spectrometer was calibrated with the Au $4f_{7/2}$ line (binding energy 83.98 eV). The analyzer energy and spot size were, respectively, 50 eV and 1.4 mm^2. These conditions give a Full Width at Half Maximum (FWHM) on Au $4f_{7/2}$ of 1 eV. The positive charge, developed on the samples due to the photoejection process, was compensated by a charge neutralizer (a flood gun) whose energy was adjusted at 6 eV (50 μA). The binding energies were calculated with respect to the C1*s* peak (C–C, C–H) set at 284.6 eV. The intensities were estimated by calculating the integral of each peak after subtraction of the "S-shaped" background (*23*). Atomic concentration ratios were calculated by correcting the intensity ratios with the theoretical sensitivity factors based on Scoffield cross sections (*24*). The transmission function of the spectrometer was assumed to be independent of the kinetic energy (Ek) and electron mean free paths (IMFP) were taken to be proportional to $(Ek)^{0.7}$. Decomposition of peaks was done with the best fitting routine of the SSI instrument.

RESULTS AND DISCUSSION

The Mechanism of Adsorption of the Molybdates on Titania

Figure 2 illustrates the variation of the electrokinetic charge, $\sigma_{e.k.}$, with pH of the support suspension in the absence and presence of molybdates (curves a and c, respectively) as well as of an MoO_3/TiO_2 catalyst suspension (curve b). It may be seen that the presence of the molybdates in the solution caused a reversal of the electrokinetic charge, rendering it negative in the whole pH range. This result precluded the location of the molybdates in the diffuse part of the double layer as counter ions, because in this case the value of $\sigma_{e.k.}$, namely the charge from the surface up to shear plane (Fig. 1), should be positive in order to compensate the negative charge of the molybdates. Two possibilities remain, therefore, for the location of the molybdates: (i) the surface of the support and (ii) the Inner Helmholtz Plane of the double layer. In the first case surface bonds should be formed between the molybdate ions and the surface hydroxyls of the support, similar to those formed after calcination in the MoO_3/TiO_2 catalysts. It is, therefore, reasonable to assume that in both suspensions similar $\sigma_{e.k.}$ vs pH curves should be obtained. Our experimental results however (compare curves c and b) clearly showed that this is not the case. Thus, the unique possibility left for the location of the molybdates is the Inner Helmholtz Plane of the double layer.

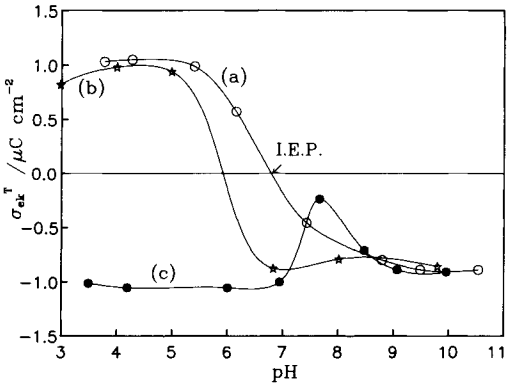

FIG. 2. Electrokinetic charge density, $\sigma_{e.k.}$, as a function of pH of the suspension at 25°C. (a) TiO_2/NH_4NO_3; (b) $MoO_3/TiO_2/NH_4NO_3$; (c) $Mo_xO_y^{z-}$ ions $/TiO_2/NH_4NO_3$, $C_0 = 1 \times 10^{-3}$ mol $Mo^{(VI)}$ dm^{-3}. $I = 0.01$ mol dm^{-3}.

The above conclusion, similar to that proposed for γ-alumina (*7*), differs from an ear-

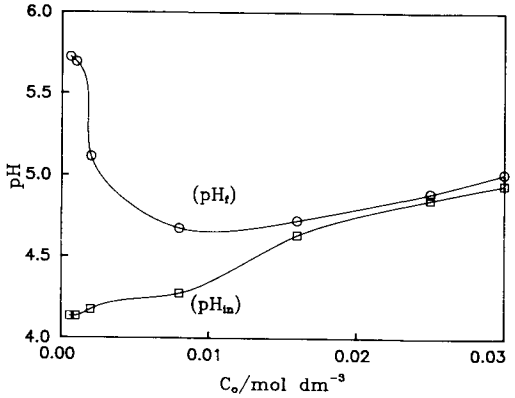

FIG. 3. Illustrates the variation in the pH measured before, pH_{in}, and after, pH_f, adsorption with C_0.

lier suggestion that the molybdates were deposited on the surface reacting with the neutral hydroxyls (*3, 5, 12–14*). This view predicted increase in the pH after adsorption and was based on the pH vs C_0 curves usually observed for γ-alumina. As we have obtained similar curves for titania (a typical example is illustrated in Fig. 3) we should discuss this point. As it has been mentioned for γ-alumina, the increase in pH after adsorption should be easily attributed to equilibria (a), when the pH of the molybdate solution is lower than the p.z.c. of titania. In this pH region the titania surface becomes positive at expense of the H_b^+ ion produced by the water dissociation.

The pH vs C_0 curves can, moreover, help us to shed more light on the mechanism of adsorption: Considering the most important equilibria existing in the molybdate solution, a critical question is raised:

$$Mo_7O_{24}^{6-} + 4H_2O \rightleftarrows 7MoO_4^{2-} + 8H_b^+ \quad (c)$$

$$Mo_7O_{24}^{6-} + MoO_4^{2-} + 2H_b^+ \rightleftarrows [H_2Mo_8O_{28}]^{6-} \quad (d)$$

Do polymolybdates first dissociate to MoO_4^{2-} before adsorption (*3, 12, 15, 27*) or are they adsorbed intact? (*1,2, 27, 28*). Inspecting equilibria (a), (c), and (d) it may be concluded that only equilibrium (c) is related with a decrease in pH upon decomposition of $Mo_7O_{24}^{6-}$. Therefore, in order to explain the decrease of the pH change, $\Delta pH = pH_f - pH_{in}$, as C_0 increased we should assume that the polymolybdates are transformed to a large extent into MoO_4^{2-} before adsorption.

Figure 4 illustrates the adsorption isotherms obtained between pH 4.6 and 9.0. It may be seen that in all cases a plateau was obtained, corresponding to the monolayer surface coverage. The experimental points are well fitted with an L-type isotherm. This type of isotherm implies localized, Langmuir-type adsorption of the molybdate ions on the IHP with very weak, if any, lateral interactions compared with those related with isotherms of S type (*7, 17*). In view of the above considerations we analyzed the isotherms obtained at various pH values. The analysis was based on the following assumptions: (i) MoO_4^{2-} ions are specifically adsorbed on the IHP, as it has been concluded in the previous paragraphs. (ii) The adsorbed MoO_4^{2-} ions are located on energetically equivalent sites, an implication of the Langmuirian shape of the isotherms obtained. (iii) One specifically adsorbed ion, replaces one water molecule from the IHP (*25*). (iv) Lateral interactions are exerted between the adsorbed molybdate ions and E is the corresponding energy (*26*).

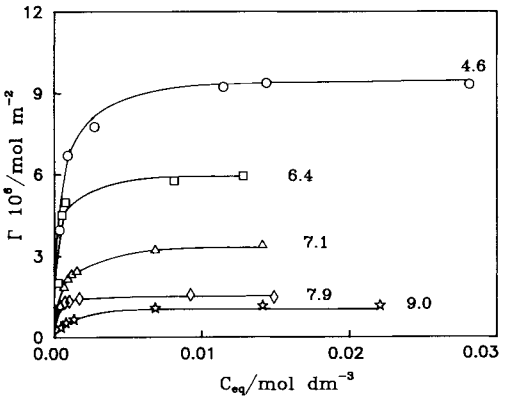

FIG. 4. Surface concentration of $Mo^{(VI)}$ as a function of the equilibrium $Mo^{(VI)}$ concentration at various pH values of the impregnating suspension. T = 25°C, I = 0.1 mol dm^{-3} NH_4NO_3. pH values are indicated.

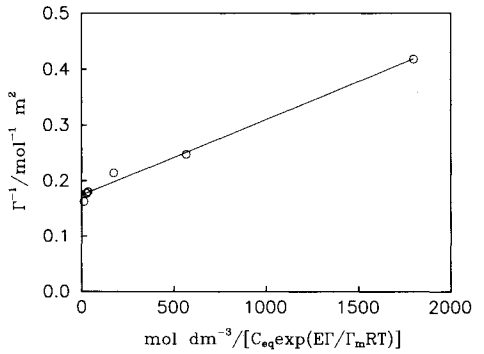

FIG. 5. Reciprocal surface concentration of $Mo^{(VI)}$ as a function of $1/C_{eq}\exp(E\Gamma/\Gamma_m RT)$. The solid line represents the values calculated using Eq. (6).

Treatment of the experimental data, in a manner analogous to the case of γ-Al_2O_3 (*7*), yielded the "Stern–Langmuir–Fowler" equation, which is an expression similar to that derived by A. de Keizer and J. Lyclema (*25*),

$$1/\Gamma = 1/\Gamma_m + 1/\Gamma_m \tilde{K} C_{eq} \exp(E\Gamma/\Gamma_m RT), \quad (6)$$

where

$$\tilde{K} = (a/55.5)\exp(-2F\Psi_\beta/RT - \Delta G^\circ_{cs}/RT). \quad (7)$$

In Eqs. (6) and (7) Γ_m, $\tilde{K}$, a, Ψ_β, and ΔG°_{cs} represent respectively the "saturation surface concentration" of the $Mo^{(VI)}$ corresponding to the monolayer, the adsorption constant, a coefficient independent from the C_{eq} but dependent on temperature and pH, the potential at the IHP, and the contribution of the chemical interactions between the adsorbed MoO_4^{2-} ions and the support, to the standard free energy of adsorption.

It was found that Eq. (6) described satisfactorily our experimental data, suggesting the existence of lateral interactions between the adsorbed ions. A typical example is illustrated in Fig. 5.

From the above considerations it was clearly shown that, as in the case of γ-alumina (*7*), the MoO_4^{2-} ions are adsorbed on energetically equivalent sites formed on the IHP. However, the L and S type of isotherms obtained in titania and γ-alumina respectively, suggested adsorbate–adsorbate interactions weak in the former case and strong in the latter. This may be confirmed by comparison of the E values obtained for the respective supports (Table 1).

TABLE 1

Values of the Lateral Interaction Energy, E, for Different Carriers at pH = 4.6 and T = 25°C; I = 0.1 mol dm^{-3} NH_4NO_3

Carrier	E (KJ mol^{-1})
γ-Al_2O_3	10.5 ± 0.3
TiO_2	2.2 ± 0.1

The variation of the Γ_m with the surface charge of TiO_2, σ_0^T, determined in the presence of molybdates, may be used to investigate the nature of the surface groups responsible for the creation of the adsorption sites on the IHP. Such a variation is illustrated in Fig. 6. It may be seen that the extent of adsorption increased with the surface charge. This strongly suggested that the deprotonated surface hydroxyls did not participate in the creation of the adsorption sites. On the other hand, on the basis of Fig. 6, the participation of the neutral hydroxyls to the creation of the adsorption sites should

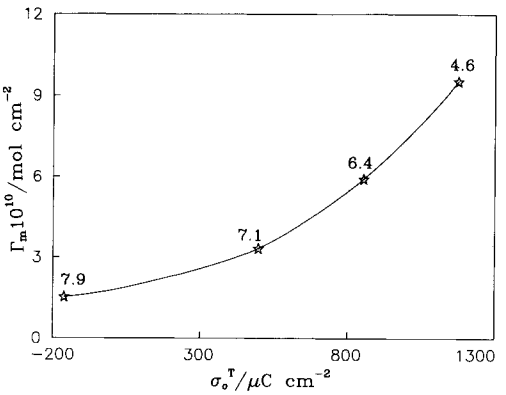

FIG. 6. Saturation surface $Mo^{(VI)}$ concentration as a function of the total surface charge density, σ_0^T.

not be precluded. In fact, at pH values higher than those corresponding to the p.z.c. (p.z.c. in the presence of molybdates at pH 7.5), where only deprotonated and neutral surface hydroxyls are practically present on the titania surface, a significant adsorption may be measured. However, the contribution of the protonated surface hydroxyls in the creation of the adsorption sites should be more important compared to that of the neutral hydroxyls. Comparison of the slopes of the lines obtained for pH values below and above the p.z.c. showed that the former were substantially higher. It should be noted that the increase in the value of the surface charge σ_0^T as pH decreased should in principle be attributed to the creation of the protonated hydroxyls. In conclusion, Fig. 6 shows that the protonated and to some extent the neutral surface hydroxyls are involved in the creation of the adsorption sites.

In view of the results presented already we tentatively propose the following mechanisms for the adsorption of the molybdates on the titania surface (see Figs. 7a and 7b). In both cases MoO_4^{2-} are located in the IHP of the double layer replacing water molecules whereas the hydrated NH_4^+ are the counter ions. The first mechanism (Fig. 7a) is more probable at relatively low concentration of the protonated surface hydroxyls ($TiOH_2^+$), namely, at relatively high pH values. At these pH values the electrokinetic charge is negative (see Fig. 2), mainly due to the relatively high concentration of the deprotonated surface hydroxyls not shown in Fig. 7a. It was therefore assumed that the NH_4^+ are the counter ions. The mechanism predicts an enhancement of the protonation of the neutral surface hydroxyls involved in the creation of the adsorption sites, in order for the MoO_4^{2-} ions to be stabilized in the IHP by forming ion pairs (*18*), as shown in Fig. 7a. In this case the amount of protons adsorbed on the support surface should be greater in the presence than in the absence of MoO_4^{2-} ions in the suspension. This may be tested by doing potentiometric titrations of selected solutions [NH_4NO_3, $NH_4NO_3/Mo_xO_y^{z-}$] and suspensions [TiO_2/NH_4NO_3, $TiO_2/Mo_xO_y^{z-}/NH_4NO_3$]. Typical titration curves obtained are shown in Fig. 8. As may be seen the hydrogen ions added in the course of the potentiometric titrations are consumed by the protonation of surface hydroxyls [equilibria (a)], as well as through their participation in other equilibria in the solutions. The rest are accumulated causing a drop of the solution pH. Evidently the difference {(a) − (b) = $H^+_{T,Mo}$} and {(c) − (d) = H^+_T} is respectively equal to the hydrogen ions consumed for the protonation of the surface hydroxyls of the support in the presence and absence of the $Mo_xO_y^{z-}$ ions in the solution. It may be noted that $H^+_{T,Mo} > H^+_T$, in excellent agreement with the mechanism drawn in Fig. 7a. The second

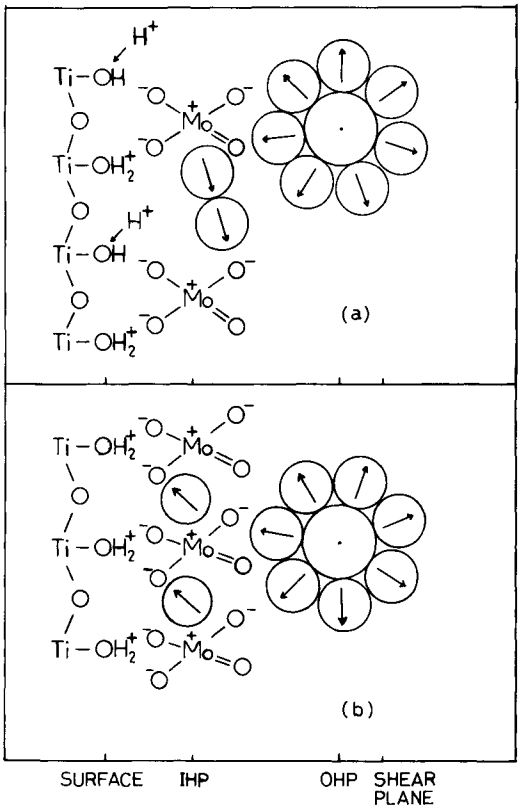

FIG. 7. The mechanisms of adsorption of the molybdates on titania. (⊖) Water dipole, (○) NH_4^+ ion. (a) Relatively high pH's. (b) Relatively low pH's.

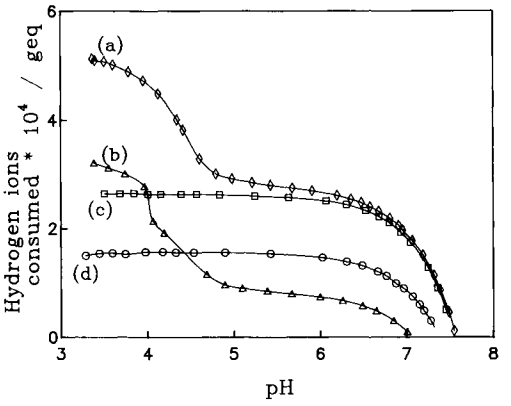

FIG. 8. Hydrogen ions consumed to the protonation of surface hydroxyls as well as to the equilibria taking place in the solution. (a) suspension $TiO_2/NH_4NO_3/Mo_xO_y^{z-}$ ions; (b) solution $NH_4NO_3/Mo_xO_y^{z-}$ ions; (c) suspension TiO_2/NH_4NO_3; (d) solution NH_4NO_3. I = 0.1 mol dm^{-3}.

mechanism (Fig. 7b) is more probable at relatively high concentration of $TiOH_2^+$, namely, at relatively low pH, where the surface charge is positive. The specific adsorption of relatively large amounts of MoO_4^{2-} in the IHP according to this mechanism explains the shift in the $\sigma_{e.k.}$ from positive to negative values (compare Figs. 2a and 2c).

Characterization of the MoO_3/TiO_2 Catalysts Prepared at Various pH Values (Table 2)

The relation between the pH_f values of the impregnating solution and the saturation surface concentration of $Mo^{(VI)}$ is shown in Fig. 9. Comparison of our results with recently reported results (*6, 9*) shows that in both cases an increase in the surface concentration took place as pH decreased. However, the curves obtained are not identical. This is presumably due to the fact that the adsorption experiments were done at different temperatures and ionic strength values (*9*). These results were explained in terms of i.e.p. of the titania (*9*). But as already mentioned this is not a surface parameter (Fig. 1). This is, in fact, the case in the $Mo^{(VI)}/TiO_2$ system where p.z.c. and i.e.p. are different. (Compare Fig. 2 with Fig. 4 of Ref. (*10*)). On the basis of the mechanistic models proposed above we may explain the increase in the value of Γ_m as pH decreased. In fact, decrease in pH causes a progressive transformation of the deprotonated to neutral and next to protonated hydroxyls which in turn promote the creation of additional adsorption sites.

Figure 10 illustrates the variation of the CO_2 and NO uptake with the $Mo^{(VI)}$ loading in terms of wt% MoO_3. As may be seen, at pH = 7.3, corresponding to about 2 wt% MoO_3, the titania surface has been completely covered and the active surface has almost reached its maximum value. This conclusion was also corroborated by the XPS results concerning these catalysts. Fig-

TABLE 2

The pH Values of the Impregnating Suspensions, the Mo Loadings, and the Specific Surface Areas of the Catalysts Prepared by the Equilibrium Adsorption Method; T = 25°C, I = 0.1 mol dm^{-3} NH_4NO_3

Number	pH	%MoO_3	SSA
1	8.3	0.9	47.9
2	7.3	2.0	45.0
3	6.5	3.5	41.6
4	4.6	5.4	43.3

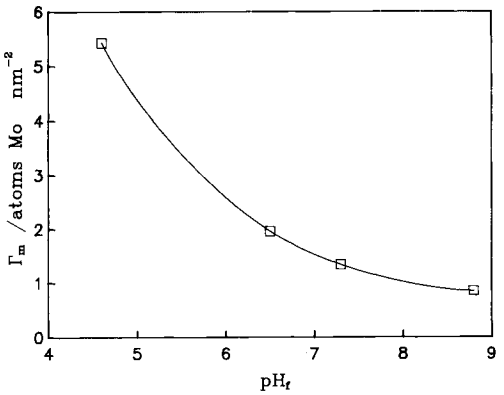

FIG. 9. Saturation surface $Mo^{(VI)}$ concentration as a function of the impregnating solution pH measured after the adsorption, pH_f.

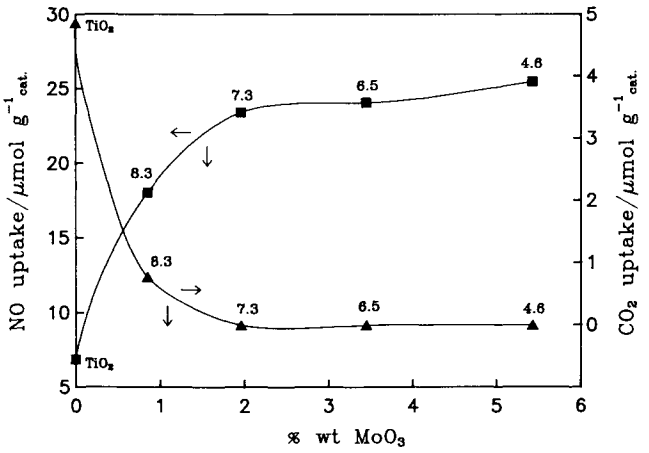

FIG. 10. Illustrates the variation in the NO and CO_2 chemisorption of the MoO_3/TiO_2 samples with the wt% MoO_3 loading.

ure 11 illustrates the variation of Mo/(Mo + Ti) atomic ratio on the surface of these samples, curve (a), with the wt% MoO_3 loading. The change in the slope of the curve (a) at MoO_3 loading between 1 and 2 wt% showed that a change in the dispersion of the molybdena phase occurred in this region. This change should be attributed to the formation of a second layer as well as to the formation of MoO_3 crystallites.

The results presented above, support the

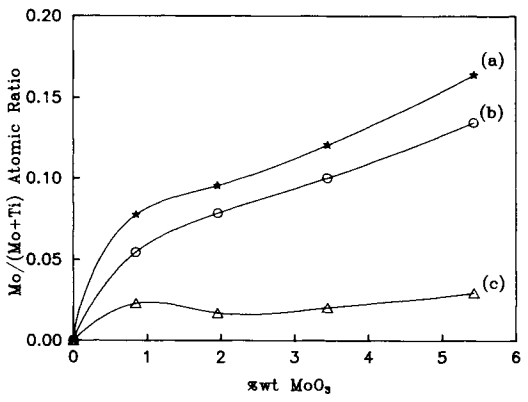

FIG. 11. Variation of the Mo/(Mo + Ti) atomic ratio on the surface with the wt% MoO_3 loading. (a) Total molybdena species; (b) molybdena species giving the high binding energy peaks; (c) molybdena species giving the low binding energy peaks.

view that the first $Mo^{(VI)}$ monolayer has been completed at about 2 wt% MoO_3. This value is lower than the theoretical MoO_3 loading required for the titania used (ca. 4 wt% MoO_3) (*6, 29*) and is far from that (6.6 wt% MoO_3) found by Kim *et al.* (*9*). We have tried to further examine this discrepancy using the Raman spectroscopy. This technique is a powerful tool for discerning between molybdenum oxide monolayers or crystallites on the titania surface. A peak found in the 940–970 cm^{-1} range has been attributed to a two-dimensional molybdenum oxide overlayer on the titania support surface (*6, 9, 29–32*), while a Raman band at 823 cm^{-1} has been considered to be characteristic of crystalline MoO_3 particles (*9, 33*). We have observed the latter peak only in the spectrum of our specimen containing 5.4% MoO_3 [see spectrum (b) in Fig. 12]. This observation showed that in our case crystalline MoO_3 has started to form in loadings lower than 6.6 wt% MoO_3, in agreement with the theoretical value for monolayer coverage. The fact that, a second layer (no MoO_3 crystallites) was mainly formed in the 2–5 wt% MoO_3 range could be presumably responsible for the absence of the Raman band at 823 cm^{-1} [Fig. 12 curve(a)], although, the monolayer coverage has been exceeded, as it has been suggested both by the NO and

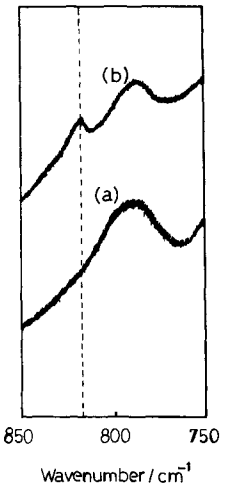

FIG. 12. Raman spectra for the MoO_3/TiO_2 samples containing: (a) 3.45 wt% MoO_3 and (b) 5.43 wt% MoO_3.

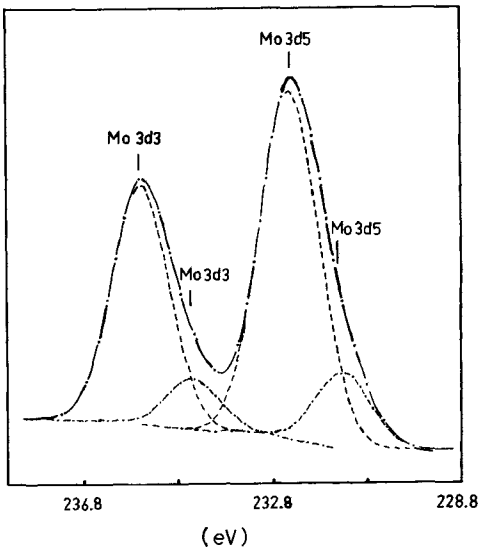

FIG. 13. Mo3d photoelectron spectrum for an MoO_3/TiO_2 species. The two kinds of peaks, one of low (----) and other of high (·····) binding energy are depicted.

CO_2 adsorption experiments as well as by the XP spectroscopy.

The chemical nature of the supported species as well as the intensity of the interactions between the supported species and the support could be studied using the binding energy and the shape of the XPS peaks. The changes observed in the binding energies of Mo $3d_{3/2}$ and Ti $2p_{3/2}$ photoelectrons which were found to be equal to 232.6 ± 0.4 and 458.7 ± 0.3 eV, respectively, were insignificant. Trying to deconvolute the Mo 3*d* double peaks of the recorded spectra, four peaks appeared in all cases, two of them under the original Mo $3d_{3/2}$ peak and the other two under the original Mo $3d_{5/2}$ peak. A typical example is shown in Fig. 13. This phenomenon was observed for the first time and probably indicated that two molybdena species were formed on the titania surface and/or two kinds of interactions exist between the support and the supported phase. In any case, the areas of the deconvoluted peaks may be used to determine the relative amounts of the two states in all samples. The results are plotted in Fig. 11 [curves (b) and (c)] as a function of the wt% MoO_3 loading. Inspection of these curves showed that the amount of the molybdena species, giving the low binding energy Mo3d peaks, was independent of the total MoO_3 contained in the samples for loadings exceeding 1 wt% MoO_3 (Fig. 11c). On the other hand, the amount of molybdena species, giving rise to the high binding energy Mo 3*d* peaks, increased with the wt% MoO_3 loading (Fig. 11b).

In order to further examine the possible existence of the two molybdena species suggested by the XPS results, TPR experiments were done and the corresponding patterns are illustrated in Fig. 14. The TPR results showed three peaks centered at about 700–800°C, 500–600°C, and 450°C. The first peak was attributed to the Mo monolayer and the second to the Mo bilayer (*34, 35*). These results showed that the formation of the bilayer started from the catalyst with the lowest Mo loading corroborating the CO_2 and NO adsorption results as well as the XPS results. In fact, a marked change in the slope of curves in Figs. 10 and 11a for the sample with the lowest Mo loading was observed.

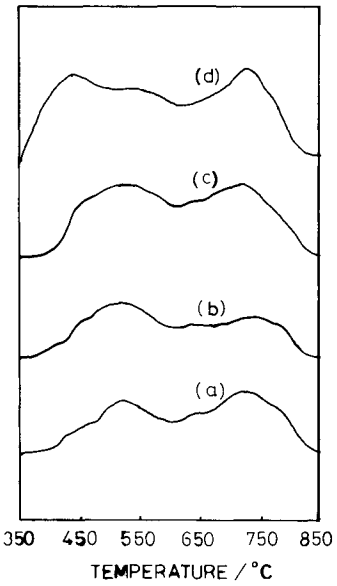

FIG. 14. TPR spectra for the MoO_3/TiO_2 samples containing: (a) 0.85, (b) 1.96, (c) 3.45, and (d) 5.43 wt% MoO_3.

The third peak at 450°C may be attributed to an Mo oxidic species with relatively low reduction temperature which presumably implies a species with relatively low "active phase-carrier" interactions and thus dispersion. This species is probably responsible for the low binding energy peaks detected for the first time by XPS. In fact, these XPS peaks were not observed in the MoO_3/γ-Al_2O_3 catalysts prepared by adsorption on which a reduction peak at 450°C did not appear (*36*). Adopting this assignment for the peak centered at about 450°C we may note that the relative amount of the formentioned species increased with the Mo loading whereas its surface remained constant (Fig. 11c) suggesting a progressive decrease in its dispersion. It seems that the amount of this Mo oxidic species became sufficient to be detected by Raman when Mo loading reached 5.4 wt% MoO_3.

Taking into account all of the results shown above we may propose the following picture for the surface structure of the MoO_3/TiO_2 catalysts prepared by adsorption; an MoO_3 monolayer forms as the MoO_3 loading increases and it fully covers the TiO_2 surface at 2 wt% MoO_3 loading. A second layer starts to form before the first is completed, the area of which increases with the MoO_3 content. A poorly dispersed Mo oxidic species forms in all specimens studied. The amount of this species increases with Mo loading and becomes sufficient to be detected by Raman when Mo loading reaches 5.4 wt% MoO_3 (Fig. 12b).

CONCLUSIONS

(i) The groups responsible for the creation of adsorption sites are the neutral but mainly the protonated surface hydroxyls of TiO_2.

(ii) The MoO_4^{2-} ions are adsorbed on the IHP of the double layer developed between the surface of the titania particles and the impregnating solution.

(iii) The adsorbed MoO_4^{2-} ions are located on energetically equivalent sites of the IHP.

(iv) Relatively weak lateral interactions are exerted between the adsorbed molybdates.

(v) The change of the sorptive capacity of TiO_2 with pH may be explained in terms of the mechanism of adsorption.

(vi) At pH = 7.3, corresponding to about 2 wt% MoO_3, the titania surface is completely covered and a second molybdena layer starts to form at pH's lower than 7.3.

(vii) A poorly dispersed Mo oxidic species formed in all specimens studied increases with Mo loading and becomes sufficient to be detected by Raman when Mo loading reaches 5.4 wt% MoO_3.

ACKNOWLEDGMENTS

We gratefully acknowledge kind help given by Mr. D. Kodaridis and Professor G. Papatheodorou in the Raman spectra acquisition and explanation.

REFERENCES

1. Wang, L., and Hall, W. K., *J. Catal.* **77,** 232 (1982).
2. Kasztelan, S., Grimblot, J., Bonnelle, J. P., Payen, E., Toulhoat, H., and Jacquin, Y., *Appl. Catal.* **7,** 91 (1983).

3. Iannibello, A., Marengo, S., Trifiro, F., and Villa, P. L., *in* "2nd International Symposium on Scientific Basis for the Preparation of Heterogeneous Catalysts, Louvain La Neuve, Belgium, 1978," paper A5.
4. Caceres, C. V., Fierro, J. L. G., Agudo, A. L., Blanco, M. N., and Thomas, H. J. , *J. Catal.* **95,** 501 (1985).
5. Van Veen, J. A. R., de Wit, H., Emeis, C. A. and Hendriks, P. A. J. M., *J. Catal.* **107,** 579 (1987).
6. Ng, K. Y. S., and Gulari, E., *J. Catal.* **92,** 340 (1985).
7. Spanos, N., Vordonis, L., Kordulis, Ch., and Lycourghiotis, A., *J. Catal.* **124,** 301 (1990).
7. Spanos, N., Vordonis, L., Kordulis, Ch., and Lycourghiotis, A., *J. Catal.* **124,** 301 (1990).
8. Segawa, K., Kim, D. S., Kurusu, Y., and Wachs, I. E., in "Proceedings, 9th International Congress on Catalysis, Calgary, 1988" (M. J. Phillips and M. Ternan, Eds.), p. 1960. Chem. Institute of Canada, Ottawa, (1988).
9. Kim, D. S., Kurusu, Y., Wachs, I. E., Hardaste, F. D., and Segawa, K., *J. Catal.* **120,** 325 (1989).
10. Akratopulu, K. Ch., Kordulis, Ch., and Lycourghiotis, A., *J. Chem. Soc. Faraday Trans.* **86**(20), 3437 (1990).
11. Lyclema, J., *in* "Solid/Liquid Dispersions," Ch. 3, p. 70. Academic Press, London, 1987.
12. Iannibello, A., and Mitchell, P. C. H., *in* "2nd International Symposium on Scientific Basis for the Preparation of Heterogeneous Catalysts, Louvain La Neuve, Belgium, 1978," paper E2.
13. Van Veen, J. A. R., and Hendriks, P. A. J. M., *Polyhedron* **5,** 75 (1985).
14. Jeziorowski, H., and Knozinger, H., *J. Phys. Chem.* **83,** 1166 (1979).
15. Houalla, M., Kibby, C. L., Petrakis, L., and Hercules, D. M., *J. Catal.* **83,** 50 (1983).
16. Vordonis, L., Koutsoukos, P. G., and Lycourghiotis, A., *J. Catal.* **98,** 286 (1986).
17. Spanos, N., Vordonis, L., Kordulis, Ch., Koutsoukos, P. G. and Lycourghiotis, A., *J. Catal.* **124,** 315 (1990).
18. Vordonis, L., Koutsoukos, P. G., and Lycourghiotis, A., *J. Catal.* **101,** 186 (1986).
19. Topsoe, N. Y., and Topsoe, H., *J. Catal.* **75,** 354 (1982).
20. Bordero, T. A., and Bartholomew, C. H., *J. Catal.* **84,**143 (1983).
21. Papadopoulou, Ch., Lycourghiotis, A., Grange, P., and Delmon, B., *Appl. Catal.* **38,** 255 (1988).
22. Lemaitre, J. L., *in* "Characterization of Heterogeneous Catalysts" (F. Delanay, Ed.) Ch. 1. Dekker, New York and Basel, 1984.
23. Shirley, D. A., *Phys. Rev.* **35,** 4709 (1972).
24. Scoffield, J. H., *J. Electron Spectrosc. Relat. Phenom.* **8,** 129 (1976).
25. de Keizer, A., and Lyclema, J., *J. Colloid Interface Sci.* **75,** 171 (1980).
26. Jaycock, M. J., and Parffit, G. D., "Chemistry of Interfaces." Wiley, New York, 1981.
27. Knozinger, H., and Jeziorowski, H., *J. Phys. Chem.* **82,** 2002 (1978).
28. Wang, L., and Hall, W. K., *J. Catal.* **66,** 251 (1980).
29. Stencel, J. M., *in* "Raman Spectroscopy for Catalysis," p. 66. Van Nostrand–Reinhold Catalysis Series, Van Nostrand–Reinhold, New York, 1990.
30. Machej, T., Haber, J., Turek, A. M., and Wachs, I. E., *Appl. Catal.* **70,** 115 (1991).
31. Liu, Y. C., Griffin, G. L., Chan, S. S. and Wachs, I. E., *J. Catal.* **94,** 108 (1985).
32. Quincy, R. B., Houlla, M. and Hercules, D. M., *J. Catal.* **106,** 85 (1987).
33. Stampfl, S. R., Chen, Y., Dumesic, J. A., Nh, C. and Hill, C. G., *J. Catal.* **105,** 445 (1987).
34. Arnoldy, P., Franken, M. C., Scheffer, B., and Moulijn, J. A., *J. Catal.* **96,** 381 (1985).
35. Thomas, R., van Oers, E. M., de Beer, V. H. J., Medema, J., and Moulijn, J. A., *J. Catal.* **76,** 241 (1982).
36. Spanos, N., "Study of the Adsorption of Catalytically Active Ions on Charged Surfaces of Industrial Carriers," Chap. 5. PhD thesis, University of Patras, Patras, Greece, 1991.